ENGINEERING TRANSACTIONS • *Engng. Trans.* • **54**, 4, 289–321, 2006
Polish Academy of Sciences • Institute of Fundamental Technological Research
10.24423/engtrans.248.2006

INVESTIGATION OF MACROCRACK PROPAGATION ALONG A BIMATERIAL INTERFACE IN ADIABATIC DYNAMIC PROCESSES AS A PROBLEM OF MESOMECHANICS

W. Dornowski, P. Perzyna

Institute of Fundamental Technological Research
Polish Academy of Sciences
Świętokrzyska 21, 00–049 Warsaw, Poland

The main objective of the present paper is the investigation of macrocrack propagation along a bimaterial interface in adiabatic dynamic processes. The investigation has been generated by very recent experimental observation (cf. ROSAKIS, SAMUDRALA and COKER [34], GUDURU, ROSAKIS and RAVICHANDRAN [13], GUDURU, ZEHNDER, ROSAKIS and RAVICHANDRAN [14]).

A general constitutive model of elastic-viscoplastic damaged polycrystalline solids has been developed within the thermodynamic framework of the rate-type covariance material structure with a finite set of internal state variables. This set of internal state variables will be assumed and interpreted so that the theory developed has been taken into account the effects as follows: (i) plastic non-normality; (ii) softening generated by microdamage mechanisms; (iii) thermomechanical coupling (thermal plastic softening and thermal expansion); (iv) strain-rate sensitivity. It is noteworthy to stress that viscosity introduces implicitly a length–scale parameter into the dynamical initial boundary value problem.

In order to describe in a constitutive model all the previously mentioned properties and incorporate their respective effects, it is intended to introduce a particular set of internal state variables, which consists of the equivalent inelastic deformation and volume fraction porosity. The equivalent inelastic deformation can describe the dissipation effects generated by viscoplastic flow phenomena and the volume fraction porosity takes into account the microdamage evolution effects. The kinetics of microdamage plays a very important role in this constitutive model. Fracture criterion based on the evolution of microdamage is assumed. The relaxation time is viewed either as a microstructural parameter to be determined from experimental observations, or as a mathematical regularization parameter. By assuming that the relaxation time tends to zero, the rate-independent elastic-plastic response can be obtained. The identification procedure is developed basing on the experimental observations.

We consider isothermal and adiabatic processes in the thin flat specimen made of two identical elements (material A) and the cohesive band (material B). The width of the cohesive band is 1 μm, so it is a mesoscale size range. In this cohesive band the initial notch is localized symmetrically. It is assumed that the boundary conditions are modelled by the speed of the upper edge of the specimen, while the lower edge is clamped. The initial conditions of the problem are homogeneous. Both materials of the specimen are modelled as elastic-viscoplastic.

A two-dimensional, plane stress, finite-difference model of the entire specimen is applied. The numerical algorithm satisfies the material objectivity, i.e. is invariant with respect to any diffeomorphism (any motion).

Particular attention is focused on the investigation of interaction of stress waves on the propagation of macrocrack within the interface band. The macrocrack-tip speed history and the evolution of the transient macrocrack-tip temperature fields are obtained.

1. Introduction

Advances in computing as well as measurement instrumentation have recently allowed for the investigation of a wider spectrum of physical phenomena in dynamic failure than it was previously possible. With increasing demand for specialized lightweight, high-strength structures, failure of inhomogeneous solids was receiving increased attention. Such inhomogeneous solids include structural composites such as bonded and sandwich structures, layered and composite materials as well as functionally graded solids. Many of such solids are composed of brittle constituents possessing substantial mismatch in wave speeds, and are bonded together with weak interfaces, which may serve as sites for catastrophic failure (cf. Rosakis and Ravichandran [32]).

Application of metals and polymers at mesoscale (a size scale that ranges from a fraction of micrometer to 100 μm) are recently multiplying rapidly. There is, the considerable experimental evidence that plastic flow and particularly, fracture phenomena in crystalline solids are inherently size-dependent over the mesoscale range. However, the conventional continuum mechanics models of inelastic deformation processes are size scale-independent. The relatively large numbers of dislocations governing plastic deformation at the micron-scale, motivate the development of a continuum theory of plasticity incorporating the size-dependence. The elastic viscoplastic theory can be developed for this purpose.

In a very recent paper by Dornowski and Perzyna [10] an analysis of the macrocrack along a bimaterial interface under dynamic adiabatic processes has been presented.

The main objective of the present paper is the investigation of the macrocrack propagation along a bimaterial interface in the case when the width of the cohesive band is of mesoscale size range.

Classical dynamic fracture theories predict the surface wave speed to be the limiting speed for propagation of in-plane cracks in homogeneous, linear elastic materials subjected to remote loading. On the other hand, the very recent experiments performed by Rosakis, Samudrala and Coker [34] have provided evidence that shearing mode conditions near a propagating crack tip drive the crack intersonic speeds, which are found to be possible even in purely homogeneous systems with only one distinct set of wave speeds.

NEEDLEMAN and ROSAKIS [21] analysed numerically the dynamic crack growth along a bimaterial interface under impact shear loading. They assumed that the material on each side of the band line is characterized by an isotropic hyperelastic constitutive relation. A cohesive surface constitutive relation is also specified that relates the tractions and displacement jumps across the bond line and that allows for the creation of a new free surface. The resistance to crack initiation and the crack speed history are predicted without invoking any additional failure criterion. A plane model of the configuration used in experimental of ROSAKIS, SAMUDRALA and COKER [34] is analyzed. Calculations were carried out for parameters characterizing a steel – PMMA bimaterial. For a sufficiently low impact velocity, the crack speed increases smoothly to the PMMA Rayleigh wave speed, whereas above a sharply defined transition impact velocity, the crack speed reaches a value somewhat smaller than the PMMA dilatation wave speed.

Section 2 is devoted to the discussion of the experimental investigations performed by ROSAKIS, SAMUDRALA and COKER [34] and GUDURU, ZEHNDER, ROSAKIS and RAVICHANDRAN [13].

In Sec. 3 a general constitutive model of elasto-viscoplastic damaged polycrystalline solids is developed within the thermodynamic framework of the rate-type covariance structure with a finite set of the internal state variables. A set of the internal state variables consists of two scalars, namely of the equivalent plastic deformation and volume fraction porosity.

The relaxation time is used as a regularization parameter. By assuming that the relaxation time tends to zero, the thermo-elasto-plastic (rate independent) response of the damaged material can be obtained. Fracture criterion based on the evolution of microdamage is formulated.

It is noteworthy to stress that viscosity introduces implicitly a length-scale parameter into the dynamical initial-boundary value problem, i.e. $l = \alpha c T_m$, where c denotes the velocity of the propagation of the elastic waves in the material, T_m is the relaxation time for mechanical disturbances and is directly related to the viscosity of the material. The proportionality factor α depends on the particular initial-boundary value problem under consideration and may also depend on the microscopic properties of the material.

Section 4 discusses the identification procedure for assumed materials of the cracked bimaterial thin specimen made of two identical elements joined by the cohesive band. The material of joint elements (material A) and the cohesive band (material B) are modelled as elasto-viscoplastic with isotropic hardening-softening effects.

In Sec. 5 the formulation of the initial-boundary value problem and its solution are presented. The finite difference method with the explicit time integration scheme (conditionally stable) is used. Particular attention is focused on the investigation of the macrocrack propagation along a bimaterial interface.

2. Experimental motivation

2.1. Evolution of crack speed

Classical dynamic fracture theories predict the surface wave speed to be the limiting speed for propagation of in-plane cracks in homogeneous, linear elastic materials subjected to remote loading. Cracks or fractures are displacement discontinuities in an otherwise intact material. On the basis of the nature of the displacement discontinuity near the crack tip, three distinct fracture modes can be defined (cf. Rosakis, Samudrala and Coker [34]): mode I, the in-plane opening mode resulting from normal separation of the crack faces (opening displacement discontinuity); mode II, the in-plane mode resulting from relative sliding of crack faces perpendicularly to the crack edge (sliding displacement discontinuity); and mode III, the anti-plane shearing mode resulting from relative out-of-plane sliding of the crack faces (tearing displacement discontinuity).

Rosakis, Samudrala and Coker [34] sought to determine experimentally whether in-plane intersonic crack growth could be obtained in laboratory specimens under remote shear loading conditions. In monolithic, prenotched laboratory specimens subjected to shear loading, after initiation from the notch tip the crack does not follow a straight path in line with the notch; it invariably kinks in the local symmetric opening direction. To make the shear crack growth possible by suppressing kinking, they introduced a weak plane ahead of the notch tip in the form of a bond between two identical pieces of isotropic material. The bonding process was carefully chosen that the constitutive properties of the bond were close to those of the bulk material. They thus constructed a material system that, although not monolithic, can be considered homogeneous with regard to its linear elastic constitutive description. However, fracture toughness along the bond line is lower, so that the material is inhomogeneous with regard to its fracture properties.

In the experimental investigation performed by Rosakis, Samudrala and Coker [34], dynamic photoelasticity was chosen for capturing the stress field near the propagation crack tip because of its ability to visualize shear waves anticipated by the intersonic crack solutions.

In Fig. 1 the dynamic photoelasticity setup is shown. A Homalite–100 (Rosakis, Samudrala and Coker [33]) specimen is subjected to asymmetric impact by a projectile fired from a high-speed gas gun. The coordinate system (x_1, x_2, x_3) is centered at the crack tip. Dimensions are given in millimeters. The specimen is 4 mm thick and the bond thickness is about 20 to 30 μm. The initial notch is 25 mm long and 2.3 mm wide. For Homalite–100, $c_L = 2200$ m/s and $c_S = 1255$ m/s. The steel projectile (length 75 mm, diameter 50 mm) im-

pacts a steel piece, which was bonded to the specimen at the impact site to prevent shattering and to induce a planar loading wave front. The compressive longitudinal wave loads the notch tip in a predominantly shear mode. The dynamic stress field produced by the loading was recorded using photoelasticity in conjunction with high-speed photography. A coherent, monochromatic, plane-polarized, collimated laser beam (diameter $\phi = 50$ mm) was transmitted through the specimen. The specimen was placed in a circular polariscope, and the resulting isochromatic fringe pattern was recorded by a rotating mirror-type high-speed camera, capable of recording 80 frames at framing rates up to 2 million frames per second.

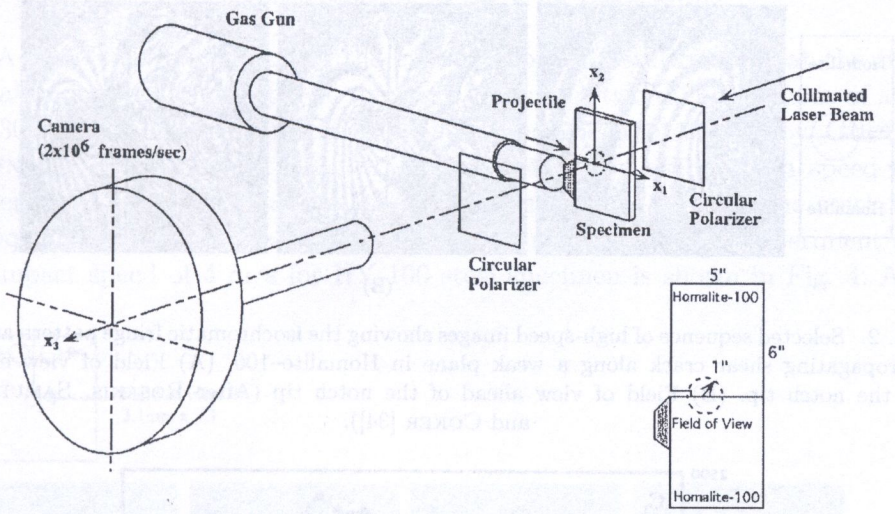

FIG. 1. The dynamic photoelasticity setup (After ROSAKIS, SAMUDRALA and COKER [34]).

The specimen was subjected to asymmetric impact loading with a projectile at 25 m/s.

Sequences of isochromatic fringe patterns were recorded around a shear crack as it initiated and propagated along the interface between two Homalite halves, cf. Fig. 2.

The frames included in the sequence are selected from two different experiments performed under identical conditions, except for the position of the field of view. Time after impact and crack tip speed are shown in each frame. The fringe pattern around the propagating crack in the last frame is similar to that in the previous frame, indicating that the propagating crack has reached a steady state.

Evolution of a crack tip speed as the mode–II crack propagates along a weak plane in Homalite–100 is presented in Fig. 3.

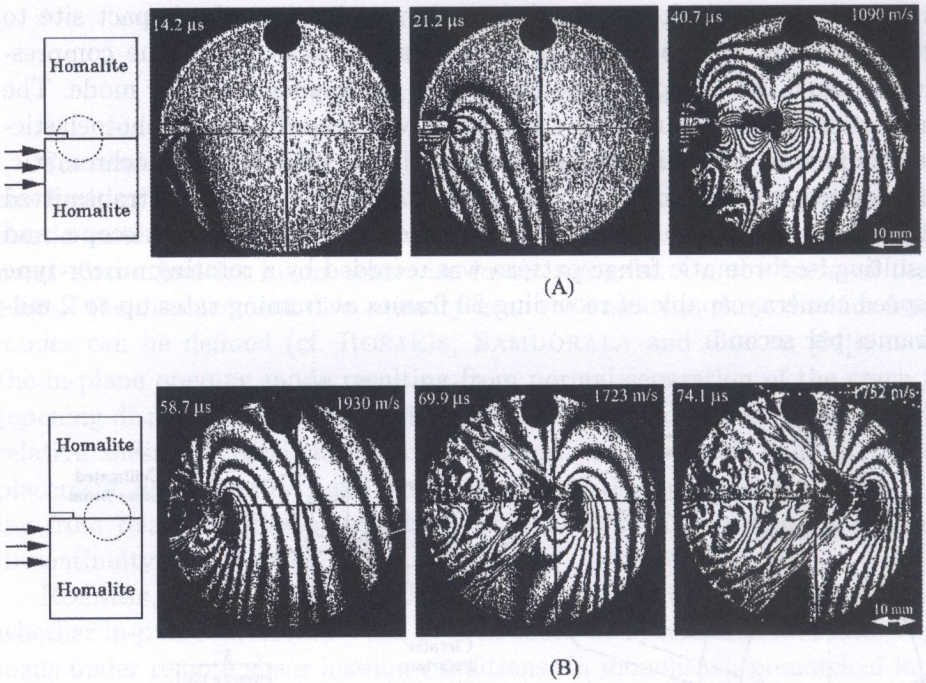

FIG. 2. Selected sequence of high-speed images showing the isochromatic fringe pattern around a propagating shear crack along a weak plane in Homalite–100. (A) Field of view enclosing the notch tip. (B) Field of view ahead of the notch tip (After ROSAKIS, SAMUDRALA and COKER [34]).

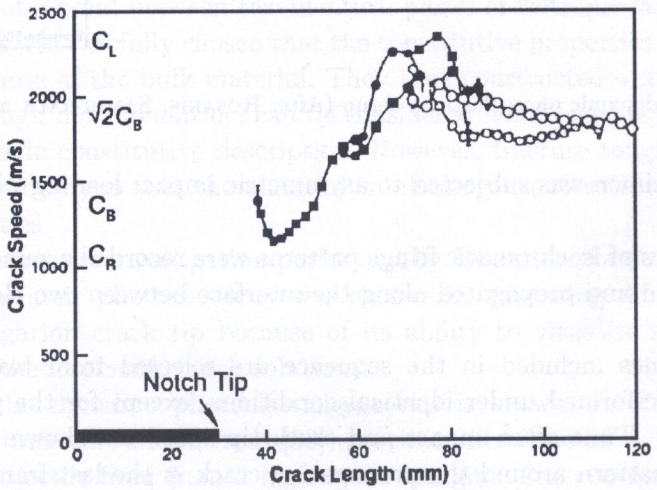

Fig. 3. Evolution of crack speed as the shear crack propagates along a weak plane in Homalite–100. Crack tip speed was obtained from crack length history (squares) and from shock wave angles (circles) for a field of view around the notch tip (solid symbols) and for a field of view ahead of the notch (open symbols) (After ROSAKIS, SAMUDRALA and COKER [34]).

From the results of Fig. 3 we see that the initially recorded crack tip is close to the shear wave speed of Homalite beyond it accelerates, thus becoming intersonic. Thereafter, it continues to accelerate up to the plane stress dilatational wave speed of Homalite, then decelerates and ultimately reaches a steady-state value of about $\sqrt{2}$ times the shear wave speed.

The experiments performed by ROSAKIS, SAMUDRALA and COKER [34] have provided evidence that shearing mode conditions near a propagating crack tip can drive the crack at intersonic speeds, what is found to be possible even in purely homogeneous systems with only one distinct set of wave speeds.

2.2. Measurements of crack tip temperature

A detailed investigation of the evolution of temperature field at the tip of a stationary crack subjected to dynamic loading in two different types of steels (C 300 maraging steel and HY 100 steel) has been presented by GUDURU, ZEHNDER, ROSAKIS and RAVICHANDRAN [14]. They used a high speed two-dimensional infrared camera to image the temperature fields at the crack tips. A sequence of thermal images obtained in the drop weight tower experiment with an impact speed of 4 m/s for HY 100 steel specimen is shown in Fig. 4. A se-

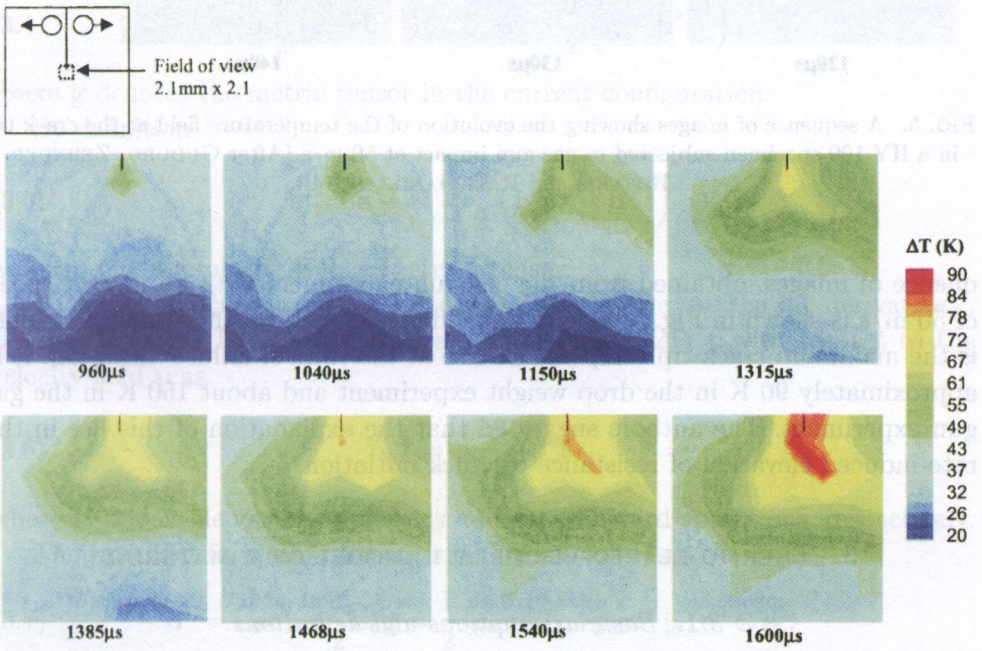

FIG. 4. A sequence of images showing the evolution of the temperature field at the crack tip in a HY 100 specimen subjected to drop weight impact at 4 m/s (After GUDURU, ZEHNDER, ROSAKIS and RAVICHANDRAN [14]).

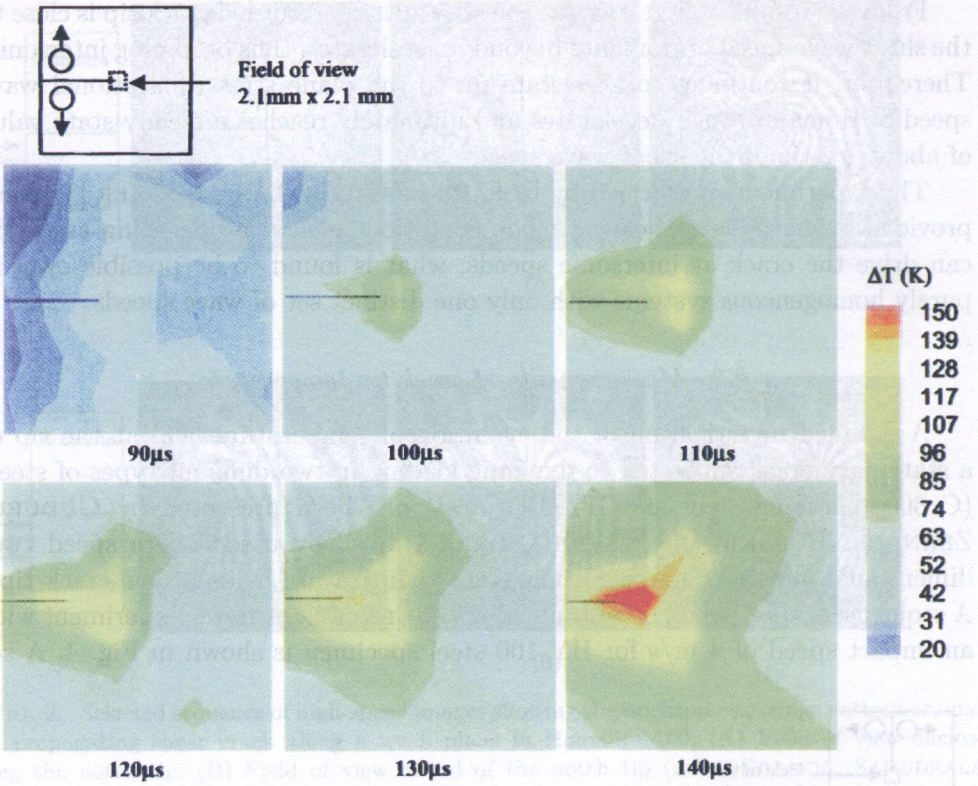

FIG. 5. A sequence of images showing the evolution of the temperature field at the crack tip in a HY 100 specimen subjected to gas gun impact at 50 m/s (After GUDURU, ZEHNDER, ROSAKIS and RAVICHANDRAN [14]).

quence of images, obtained from the gas gun experiment with an impact speed of 50 m/s is shown in Fig. 5. One major difference between the two experiments is the maximum crack tip temperature rise at the time of failure initiation. It is approximately 90 K in the drop weight experiment and about 150 K in the gas gun experiment. The authors suggested that the explanation of this lies in the rate-induced elevation of resistance to crack initiation.

3. THERMO-ELASTO-VISCOPLATIC MODEL OF A MATERIAL

3.1. Basic assumptions and definitions

Let us assume that a continuum body is an open bounded set $\mathcal{B} \subset I\!R^3$, and let $\phi : \mathcal{B} \to \mathcal{S}$ be a C^1 configuration of $\mathcal{B}$ in $\mathcal{S}$. The tangent of ϕ is denoted $\mathbf{F} = T\phi$ and is called the deformation gradient of ϕ.

Let $\{X^A\}$ and $\{x^a\}$ denote coordinate systems on $\mathcal{B}$ and $\mathcal{S}$ respectively. Then we refer to $\mathcal{B} \subset I\!R^3$ as the reference configuration of a continuum body with particles $X \in \mathcal{B}$ and to $\mathcal{S} = \phi(\mathcal{B})$ as the current configuration with points $\mathbf{x} \in \mathcal{S}$. The matrix $\mathbf{F}(\mathbf{X}, t) = \partial\phi(\mathbf{X}, t)/\partial\mathbf{X}$ with respect to the coordinate bases $\mathbf{E}_A(\mathbf{X})$ and $\mathbf{e}_a(\mathbf{x})$ is given by

$$F^a_A(\mathbf{X}, t) = \frac{\partial \phi^a}{\partial X^A}(\mathbf{X}, t), \tag{3.1}$$

where the mapping $\mathbf{x} = \phi(\mathbf{X}, t)$ represents a motion of a body $\mathcal{B}$.

We consider the local multiplicative decomposition

$$\mathbf{F} = \mathbf{F}^e \cdot \mathbf{F}^p, \tag{3.2}$$

where $(\mathbf{F}^e)^{-1}$ is the deformation gradient that releases elastically the stress on the neighbourhood $\phi(\mathcal{N}(\mathbf{X}))$ in the current configuration.

Let us define the total and elastic Finger deformation tensors

$$\mathbf{b} = \mathbf{F} \cdot \mathbf{F}^T, \qquad \mathbf{b}^e = \mathbf{F}^e \cdot \mathbf{F}^{eT}, \tag{3.3}$$

respectively, and the Eulerian strain tensors as follows

$$\mathbf{e} = \frac{1}{2}\left(\mathbf{g} - \mathbf{b}^{-1}\right), \qquad \mathbf{e}^e = \frac{1}{2}\left(\mathbf{g} - \mathbf{b}^{e^{-1}}\right), \tag{3.4}$$

where $\mathbf{g}$ denotes the metric tensor in the current configuration.

By definition[1)]

$$\mathbf{e}^p = \mathbf{e} - \mathbf{e}^e = \frac{1}{2}\left(\mathbf{b}^{e^{-1}} - \mathbf{b}^{-1}\right) \tag{3.5}$$

we introduce the plastic Eulerian strain tensor.

To define objective rates for vectors and tensors we use the Lie derivative[2)]. Let us define the Lie derivative of a spatial tensor field $\mathbf{t}$ with respect to the velocity field $\boldsymbol{\upsilon}$ as

$$\mathrm{L}_{\boldsymbol{\upsilon}}\mathbf{t} = \phi_* \frac{\partial}{\partial t}\left(\phi^* \mathbf{t}\right), \tag{3.6}$$

where ϕ^* and ϕ_* denote the pull-back and push-forward operations, respectively.

The rate of deformation tensor is defined as follows

$$\mathbf{d}^\flat = \mathrm{L}_{\boldsymbol{\upsilon}}\mathbf{e}^\flat = \frac{1}{2}\mathrm{L}_{\boldsymbol{\upsilon}}\mathbf{g} = \frac{1}{2}\left(g_{ac}\upsilon^c\,|_b + g_{cb}\upsilon^c\,|_a\right)\mathbf{e}^a \otimes \mathbf{e}^b, \tag{3.7}$$

[1)] For precise definition of the finite elasto-plastic deformation see PERZYNA [30].

[2)] The algebraic and dynamic interpretations of the Lie derivative have been presented by ABRAHAM *et al.* [1], cf. also MARSDEN and HUGHES [20].

where the symbol $\flat$ denotes the index lowering operator and $\otimes$ the tensor product,

$$v^a\,|_b = \frac{\partial v^a}{\partial x^b} + \gamma^a_{bc} v^c, \tag{3.8}$$

and γ^a_{bc} denotes the Christoffel symbol for the general coordinate systems $\{x^a\}$. The components of the spin $\boldsymbol{\omega}$ are given by

$$\omega_{ab} = \frac{1}{2}\left(g_{ac} v^c\,|_b - g_{cb} v^c\,|_a\right) = \frac{1}{2}\left(\frac{\partial v_a}{\partial x^b} - \frac{\partial v_b}{\partial x^a}\right). \tag{3.9}$$

Similarly

$$\mathbf{d}^{e^\flat} = \mathrm{L}_{\boldsymbol{v}} \mathbf{e}^{e^\flat}, \qquad \mathbf{d}^{p^\flat} = \mathrm{L}_{\boldsymbol{v}} \mathbf{e}^{p^\flat}, \tag{3.10}$$

and

$$\mathbf{d} = \mathbf{d}^e + \mathbf{d}^p. \tag{3.11}$$

Let $\boldsymbol{\tau}$ denote the Kirchhoff stress tensor related to the Cauchy stress tensor $\boldsymbol{\sigma}$ by

$$\boldsymbol{\tau} = J\boldsymbol{\sigma} = \frac{\rho_{\mathrm{Ref}}}{\rho}\boldsymbol{\sigma}, \tag{3.12}$$

where the Jacobian J is the determinant of the linear transformation $\mathbf{F}(\mathbf{X}, t) = (\partial/\partial X)\phi(\mathbf{X}, t)$, $\rho_{\mathrm{Ref}}(\mathbf{X})$ and $\rho(\mathbf{x}, t)$ denote the mass density in the reference and current configuration, respectively.

The Lie derivative of the Kirchhoff stress tensor $\boldsymbol{\tau} \in \mathbf{T}^2(\mathcal{S})$ (elements of $\mathbf{T}^2(\mathcal{S})$ are called tensors on $\mathcal{S}$, contravariant of order 2) gives

$$\mathrm{L}_{\boldsymbol{v}}\boldsymbol{\tau} = \phi_* \frac{\partial}{\partial t}(\phi^* \boldsymbol{\tau}) = \left\{\mathbf{F} \cdot \frac{\partial}{\partial t}\left[\mathbf{F}^{-1} \cdot (\boldsymbol{\tau} \circ \phi) \cdot \mathbf{F}^{-1^T}\right] \cdot \mathbf{F}^T\right\} \circ \phi^{-1} \tag{3.13}$$

$$= \dot{\boldsymbol{\tau}} - (\mathbf{d} + \boldsymbol{\omega}) \cdot \boldsymbol{\tau} - \boldsymbol{\tau} \cdot (\mathbf{d} + \boldsymbol{\omega})^T,$$

where $\circ$ denotes the composition of mappings. In the coordinate system (3.13) reads

$$(\mathrm{L}_{\boldsymbol{v}}\boldsymbol{\tau})^{ab} = F^a_A \frac{\partial}{\partial t}\left(F^{-1^A}_c \tau^{cd} F^{-1^B}_d\right) F^b_B \tag{3.14}$$

$$= \frac{\partial \tau^{ab}}{\partial t} + \frac{\partial \tau^{ab}}{\partial x^c} v^c - \tau^{cb}\frac{\partial v^a}{\partial x^c} - \tau^{ac}\frac{\partial v^b}{\partial x^c}.$$

Equation (3.14) defines the Oldroyd rate of the Kirchhoff stress tensor $\boldsymbol{\tau}$ (cf. OLDROYD [23]).

3.2. Constitutive postulates

Let us assume that: (i) conservation of mass, (ii) balance of momentum, (iii) balance of moment of momentum, (iv) balance of energy, (v) entropy production inequality-hold.

We introduce the four fundamental postulates:

(i) Existence of the free energy function. It is assumed that the free energy function is given by

$$\psi = \hat{\psi}(\mathbf{e}, \mathbf{F}, \vartheta; \boldsymbol{\mu}), \tag{3.15}$$

where $\mathbf{e}$ denotes the Eulerian strain tensor, $\mathbf{F}$ is deformation gradient, ϑ temperature and $\boldsymbol{\mu}$ denotes a set of the internal state variables.

To extend the domain of the description of the material properties, and particularly, to take into consideration different dissipation effects we have to introduce the internal state variables represented by the vector $\boldsymbol{\mu}$.

(ii) Axiom of objectivity (spatial covariance). The constitutive structure should be invariant with respect to any diffeomorphism (any motion) $\xi : \mathcal{S} \to \mathcal{S}$ (cf. MARSDEN and HUGHES [20]). Assuming that $\xi : \mathcal{S} \to \mathcal{S}$ is a regular, orientation preserving map transforming $\mathbf{x}$ into $\mathbf{x}'$ and $T\xi$ is an isometry from $T_{\mathbf{x}}\mathcal{S}$ to $T_{\mathbf{x}'}\mathcal{S}$, we obtain the axiom of material frame indifference (cf. TRUESDELL and NOLL [38]).

(iii) The axiom of the entropy production. For any regular motion of a body $\mathcal{B}$ the constitutive functions are assumed to satisfy the reduced dissipation inequality

$$\frac{1}{\rho_{\mathrm{Ref}}}\boldsymbol{\tau} : \mathbf{d} - (\eta\dot{\vartheta} + \dot{\psi}) - \frac{1}{\rho\vartheta}\mathbf{q} \cdot \mathrm{grad}\vartheta \geq 0, \tag{3.16}$$

where ρ_{Ref} and ρ denote the mass density in the reference and actual configuration, respectively, $\boldsymbol{\tau}$ is the Kirchhoff stress tensor, $\mathbf{d}$ the rate of deformation, η is the specific (per unit mass) entropy, and $\mathbf{q}$ denotes the heat flow vector field. MARSDEN and HUGHES [20] proved that the reduced dissipation inequality (3.16) is equivalent to the entropy production inequality first introduced by COLEMAN and NOLL [3] in the form of the Clausius–Duhem inequality. In fact the Clausius–Duhem inequality gives a statement of the second law of thermodynamics within the framework of mechanics of continuous media, cf. DUSZEK and PERZYNA [11].

(iv) The evolution equation for the internal state variable vector $\boldsymbol{\mu}$ is assumed in the form as follows:

$$\mathrm{L}_{\upsilon}\boldsymbol{\mu} = \hat{\mathbf{m}}(\mathbf{e}, \mathbf{F}, \vartheta, \boldsymbol{\mu}), \tag{3.17}$$

where the evolution function $\hat{\mathbf{m}}$ has to be based on careful physical interpretation of a set of the internal state variables and analysis of available experimental observations.

The determination of the evolution function $\hat{\mathbf{m}}$ (in practice a finite set of the evolution functions) appears to be the main problem of the modern constitutive modelling.

The main objective is to develop the rate-type constitutive structure for an elastic-viscoplastic material in which the effects of the plastic non-normality, micro-damage mechanism and thermomechanical coupling are taken into consideration. To do this it is sufficient to assume a finite set of the internal state variables. For our practical purposes it is sufficient to assume that the internal state vector $\boldsymbol{\mu}$ has the form

$$\boldsymbol{\mu} = (\in^p, \xi), \tag{3.18}$$

where $\in^p$ is the equivalent viscoplastic deformation, i.e.

$$\in^p = \int_0^t \left(\frac{2}{3}\mathbf{d}^p : \mathbf{d}^p\right)^{1/2} dt, \tag{3.19}$$

and ξ is the volume fraction porosity and takes account of micro-damage effects.

Let us introduce the plastic potential function $f = f(J_1, J_2, \vartheta, \boldsymbol{\mu})$, where J_1, J_2 denote the first two invariants of the Kirchhoff stress tensor $\boldsymbol{\tau}$.

Let us postulate the evolution equations as follows:

$$\mathbf{d}^p = \Lambda \mathbf{P}, \qquad \dot{\xi} = \Xi, \tag{3.20}$$

where for elasto–viscoplastic model of a material we assume (cf. PERZYNA [24–26, 30])

$$\Lambda = \frac{1}{T_m}\left\langle \Phi\left(\frac{f}{\kappa} - 1\right)\right\rangle, \tag{3.21}$$

T_m denotes the relaxation time for mechanical disturbances, the isotropic work–hardening–softening function κ is

$$\kappa = \hat{\kappa}(\in^p, \vartheta, \xi), \tag{3.22}$$

Φ is the empirical overstress function, the bracket $\langle\cdot\rangle$ defines the ramp function,

$$\mathbf{P} = \left.\frac{\partial f}{\partial \boldsymbol{\tau}}\right|_{\xi=\text{const}} \left(\left\|\frac{\partial f}{\partial \boldsymbol{\tau}}\right\|\right)^{-1}, \tag{3.23}$$

Ξ denotes the evolution function which has to be determined.

3.3. *Intrinsic micro-damage mechanisms*

To take into consideration experimentally observed time dependent effects it is advantageous to use the proposition of the description of the intrinsic micro–damage process presented by PERZYNA [28, 29] and DUSZEK–PERZYNA and PERZYNA [12].

Let us assume that the intrinsic micro-damage process consists of the nucleation and growth mechanism[3].

Physical considerations (cf. CURRAN *et al.* [4] and Perzyna [28, 29]) have shown that the nucleation of microvoids in dynamic loading processes which are characterized by very short time duration is governed by the thermally-activated mechanism. Based on this heuristic suggestion and taking into account the influence of the stress triaxiality on the nucleation mechanism we postulate for rate-dependent plastic flow[4]

$$\left(\dot{\xi}\right)_{\text{nucl}} = \frac{1}{T_m} h^*(\xi,\vartheta)\left[\exp\frac{m^*(\vartheta)\mid \tilde{I}_n - \tau_n(\xi,\vartheta,\in^p)\mid}{k\vartheta} - 1\right], \tag{3.24}$$

where k denotes the Boltzmann constant, $h^*(\xi,\vartheta)$ represents a void nucleation material function which is introduced to take account of the effect of microvoid interaction, $m^*(\vartheta)$ is a temperature-dependent coefficient, $\tau_n(\xi,\vartheta,\in^p)$ is the porosity, temperature and equivalent plastic strain-dependent threshold stress for microvoid nucleation,

$$I_n = a_1 J_1 + a_2\sqrt{J_2'} + a_3\left(J_3'\right)^{1/3} \tag{3.25}$$

defines the stress intensity invariant for nucleation, a_i $(i = 1,2,3)$ are the material constants, J_1 denotes the first invariant of the Kirchhoff stress tensor $\boldsymbol{\tau}$, J_2' and J_3' are the second and third invariants of the stress deviator $\boldsymbol{\tau}'$.

For the growth mechanism we postulate (cf. JOHNSON [15]; PERZYNA [28, 29]; PERZYNA and DRABIK [31] and DORNOWSKI and PERZYNA [8, 9])

$$\left(\dot{\xi}\right)_{\text{grow}} = \frac{1}{T_m}\frac{g^*(\xi,\vartheta)}{\kappa_0}\left[I_g - \tau_{eq}(\xi,\vartheta,\in^p)\right], \tag{3.26}$$

[3] Recent experimental observation results (cf. SHOCKEY *et al.* [36]) have shown that coalescence mechanism can be treated as nucleation and growth process on a smaller scale. This conjecture simplifies very much the description of the intrinsic micro-damage process by taking account only of the nucleation and growth mechanisms.

[4] An analysis of the experimental observations for cycle fatigue damage mechanics at high temperature of metals performed by SIDEY and COFFIN [37] suggests that the intrinsic micro-damage process does very much depend on the strain rate effects, the wave shape effects as well as on the stress triaxiality.

where $T_m\kappa_0$ denotes the dynamic viscosity of a material, $g^*(\xi,\vartheta)$ represents a void growth material function and takes account of void interaction, $\tau_{eq}(\xi,\vartheta,\in^p)$ is the porosity, temperature and equivalent plastic strain-dependent void growth threshold stress,

$$I_g = b_1 J_1 + b_2\sqrt{J_2'} + b_3\left(J_3'\right)^{1/3}, \tag{3.27}$$

defines the stress intensity invariant for growth and b_i $(i=1,2,3)$ are the material constants.

Finally the evolution equation for the porosity ξ has the form

$$\dot{\xi} = \frac{h^*(\xi,\vartheta)}{T_m}\left[\exp\frac{m^*(\vartheta)\mid I_n - \tau_n(\xi,\vartheta,\in^p)\mid}{k\vartheta} - 1\right] + \frac{g^*(\xi,\vartheta)}{T_m\kappa_0}\left[I_g - \tau_{eq}(\xi,\vartheta,\in^p)\right]. \tag{3.28}$$

This determines the evolution function Ξ.

3.4. Thermodynamic restrictions and rate type constitutive equations

Suppose the axiom of the entropy production holds. Then the constitutive assumption (3.15) and the evolution equations (3.20) lead to the results as follows

$$\boldsymbol{\tau} = \rho_{\mathrm{Ref}}\frac{\partial\hat{\psi}}{\partial\mathbf{e}}, \qquad \eta = -\frac{\partial\hat{\psi}}{\partial\vartheta}, \qquad -\frac{\partial\hat{\psi}}{\partial\boldsymbol{\mu}}\cdot \mathrm{L}_{\upsilon}\boldsymbol{\mu} - \frac{1}{\rho\vartheta}\mathbf{q}\cdot\mathrm{grad}\vartheta \geq 0. \tag{3.29}$$

The rate of internal dissipation is determined by

$$\vartheta\hat{i} = -\frac{\partial\hat{\psi}}{\partial\boldsymbol{\mu}}\cdot\mathrm{L}_{\upsilon}\boldsymbol{\mu} = -\left(\frac{\partial\hat{\psi}}{\partial\in^p}\sqrt{\frac{2}{3}}\right)\Lambda - \frac{\partial\hat{\psi}}{\partial\xi}\Xi. \tag{3.30}$$

Operating on the stress relation $(3.29)_1$ with the Lie derivative and keeping the internal state vector constant, we obtain (cf. DUSZEK–PERZYNA and PERZYNA [12])

$$\mathrm{L}_{\upsilon}\boldsymbol{\tau} = \mathcal{L}^e : \mathbf{d} - \mathcal{L}^{th}\dot{\vartheta} - [(\mathcal{L}^e + \mathbf{g}\boldsymbol{\tau} + \boldsymbol{\tau}\mathbf{g}) : \mathbf{P}]\frac{1}{T_m}\left\langle\Phi\left(\frac{f}{\kappa} - 1\right)\right\rangle, \tag{3.31}$$

where

$$\mathcal{L}^e = \rho_{\mathrm{Ref}}\frac{\partial^2\hat{\psi}}{\partial\mathbf{e}^2}, \qquad \mathcal{L}^{th} = -\rho_{\mathrm{Ref}}\frac{\partial^2\hat{\psi}}{\partial\mathbf{e}\partial\vartheta}. \tag{3.32}$$

Substituting $\dot{\psi}$ into the energy balance equation and taking into account the results $(3.29)_3$ and (3.30) we obtain

$$\rho\vartheta\dot{\eta} = -\mathrm{div}\mathbf{q} + \rho\vartheta\hat{i}. \tag{3.33}$$

Operating on the entropy relation $(3.29)_2$ with the Lie derivative and substituting the result into (3.33), we obtain

$$\rho c_p\dot{\vartheta} = -\mathrm{div}\mathbf{q} + \vartheta\frac{\rho}{\rho_{\mathrm{Ref}}}\frac{\partial\boldsymbol{\tau}}{\partial\vartheta} : \mathbf{d} + \rho\chi^*\boldsymbol{\tau} : \mathbf{d}^p + \rho\chi^{**}\dot{\xi}, \tag{3.34}$$

where the specific heat

$$c_p = -\vartheta\frac{\partial^2\hat{\psi}}{\partial\vartheta^2} \tag{3.35}$$

and the irreversibility coefficients χ^* and χ^{**} are determined by

$$\begin{aligned}
\chi^* &= -\left(\frac{\partial\hat{\psi}}{\partial\,\in^p} - \vartheta\frac{\partial^2\hat{\psi}}{\partial\vartheta\partial\,\in^p}\right)\sqrt{\frac{2}{3}}\frac{1}{\boldsymbol{\tau} : \mathbf{P}}, \\
\chi^{**} &= -\left(\frac{\partial\hat{\psi}}{\partial\xi} - \vartheta\frac{\partial^2\hat{\psi}}{\partial\vartheta\partial\xi}\right).
\end{aligned} \tag{3.36}$$

So, a set of the constitutive equations of the rate type has the form as follows

$$\begin{aligned}
\mathrm{L}_{\upsilon}\boldsymbol{\tau} &= \mathcal{L}^e : \mathbf{d} - \mathcal{L}^{th}\dot{\vartheta} - \Big[(\mathcal{L}^e + \mathbf{g}\boldsymbol{\tau} + \boldsymbol{\tau}\mathbf{g}) : \mathbf{P}\Big]\frac{1}{T_m}\left\langle\Phi\left(\frac{f}{\kappa} - 1\right)\right\rangle, \\
\rho c_p\dot{\vartheta} &= -\mathrm{div}\mathbf{q} + \vartheta\frac{\rho}{\rho_{\mathrm{Ref}}}\frac{\partial\boldsymbol{\tau}}{\partial\vartheta} : \mathbf{d} + \rho\chi^*\frac{1}{T_m}\left\langle\Phi\left(\frac{f}{\kappa} - 1\right)\right\rangle\boldsymbol{\tau} : \mathbf{P} + \rho\chi^{**}\dot{\xi}, \\
\dot{\xi} &= \frac{h^*(\xi,\vartheta)}{T_m}\left[\exp\frac{m^*(\vartheta)\mid I_n - \tau_n(\xi,\vartheta,\in^p)\mid}{k\vartheta} - 1\right] \\
&\qquad + \frac{g^*(\xi,\vartheta)}{T_m\kappa_0}\Big[I_g - \tau_{eq}(\xi,\vartheta,\in^p)\Big].
\end{aligned} \tag{3.37}$$

All the material functions and the material constants should be identified based on the available experimental data.

3.5. *Fracture criterion based on the evolution of micro-damage*

We base the fracture criterion on the evolution of the porosity internal state variable ξ. The volume fraction porosity ξ takes account of microdamage effects.

Let us assume that for $\xi = \xi^F$ catastrophe takes place (cf. PERZYNA [27]), that is

$$\kappa = \hat{\kappa}(\in^p, \vartheta, \xi)|_{\xi=\xi^F} = 0. \tag{3.38}$$

It means that for $\xi = \xi^F$ the material loses its carrying capacity. The condition (3.38) describes the main feature observed experimentally that the load tends to zero at the fracture point. The critical value of porosity ξ^F is usually determined from structural metallurgical investigation of a material.

It is noteworthy that the isotropic hardening-softening material function $\hat{\kappa}$ proposed in Eq. (3.22) should satisfy the fracture criterion (3.38).

3.6. *Length-scale sensitivity of the constitutive model*

The constitutive equations for a thermo-elastic-viscoplastic model introduce implicitly a length-scale parameter into the dynamic initial-boundary value problem, i.e.

$$l = \alpha c T_m, \tag{3.39}$$

where T_m is the relaxation time for mechanical disturbances, and is directly related to the viscosity of the material, c denotes the velocity of propagation of the elastic waves in the problem under consideration, and the proportionality factor α depends on the particular initial-boundary value problem and may also be conditioned on the microscopic properties of the material.

The relaxation time T_m can be viewed either as a microstructural parameter to be determined from experimental observations or as a mathematical regularization parameter.

To go deeply into length-scale sensitivity of the constitutive model, let us consider one-dimensional longitudinal wave propagation for an elastic-viscoplastic material. The constitutive equations are assumed in the form as follows

$$\dot{\in} P = \dot{\in} - \frac{\dot{\sigma}}{E}, \qquad \dot{\sigma} = h\dot{\in}^P + \frac{\sigma_0}{\gamma}\frac{\partial \dot{\in}^P}{\partial t}, \tag{3.40}$$

where γ denotes the viscosity parameter, σ_0 the yield stress and h the hardening-softening parameter.

The wave equation takes the form

$$\zeta\left(\frac{1}{c^2}\frac{\partial^2 \vartheta}{\partial t^2} - \frac{\partial^3 \vartheta}{\partial x^2 \partial t}\right) + \frac{E+h}{c^2}\frac{\partial^2 \vartheta}{\partial t^2} - h\frac{\partial^2 \vartheta}{\partial x^2} = 0, \tag{3.41}$$

where

$$\zeta = \frac{\sigma_0}{\gamma} = \sigma_0 T_m \tag{3.42}$$

denotes the macroscopic viscosity (or dynamic viscosity) and $c = (E/\rho)^{1/2}$.

For $\gamma \to \infty \Rightarrow \zeta \to 0$ (3.41) reduces to the wave equation for an elastic-plastic rate-independent material. To investigate the dispersive nature of wave propagation in an elastic-viscoplastic medium, a general solution for a single linear harmonic wave with angular frequency ω and wave number k is assumed

$$\vartheta = Ae^{e(kx-\omega t)}, \qquad k = \frac{2\pi}{\lambda}, \tag{3.43}$$

and A denotes the amplitude.

To satisfy the Eq. (3.41), k and ω have to be related by the dispersion relation

$$\zeta\left(\frac{1}{c^2}\omega^3 - k^2\omega\right)i - \frac{E+h}{c^2}\omega^2 + hk^2 = 0. \tag{3.44}$$

By sophisticated analysis of the dispersion relation (3.44) we can obtain the result for the internal length-scale parameter

$$l = \frac{2\sigma_0}{E} c T_m. \tag{3.45}$$

Comparison of (3.45) with (3.39) gives

$$\alpha = \frac{2\sigma_0}{E} \tag{3.46}$$

for the one-dimensional longitudinal wave propagation problem.

4. Identification procedure

4.1. Assumption of the material functions for an adiabatic process

To do the proper identification procedure we first make assumption of the material functions (cf. Dornowski and Perzyna [8]).

The plastic potential function f is assumed in the form (cf. Perzyna [27] and Shima and Oyane [35])

$$f = \left\{J_2' + [n_1(\vartheta) + n_2(\vartheta)\xi]\, J_1^2\right\}^{1/2} \tag{4.1}$$

where

$$n_1(\vartheta) = 0, \qquad n_2(\vartheta) = n = \text{const}. \tag{4.2}$$

The isotropic work-hardening-softening function κ is postulated as (cf. PERZYNA [28] and NEMES and EFTIS [22])

$$\kappa = \hat{\kappa}(\in^p, \vartheta, \xi) \tag{4.3}$$
$$= \left\{\kappa_s(\vartheta) - [\kappa_s(\vartheta) - \kappa_0(\vartheta)] \exp\left[-\delta(\vartheta) \in^p\right]\right\}\left[1 - \left(\frac{\xi}{\xi_F}\right)^{\beta(\vartheta)}\right],$$

where

$$\kappa_s(\vartheta) = \kappa_s^* - \kappa_s^{**}\overline{\vartheta}, \qquad \kappa_0(\vartheta) = \kappa_0^* - \kappa_0^{**}\overline{\vartheta},$$
$$\delta(\vartheta) = \delta^* - \delta^{**}\overline{\vartheta}, \qquad \beta(\vartheta) = \beta^* - \beta^{**}\overline{\vartheta}, \qquad \overline{\vartheta} = \frac{\vartheta - \vartheta_0}{\vartheta_0}. \tag{4.4}$$

The overstress function $\Phi\left(\frac{f}{\kappa} - 1\right)$ is assumed in the form

$$\Phi\left(\frac{f}{\kappa} - 1\right) = \left(\frac{f}{\kappa} - 1\right)^m. \tag{4.5}$$

The evolution equation for the porosity ξ is postulated as

$$\dot{\xi} = \dot{\xi}_{\text{grow}} = \frac{g^*(\xi, \vartheta)}{T_m \kappa_0(\vartheta)}\left[I_g - \tau_{eq}(\xi, \vartheta, \in^p)\right] \tag{4.6}$$

where (cf. DORNOWSKI [5])

$$g^*(\xi, \vartheta) = c_1(\vartheta)\frac{\xi}{1 - \xi},$$
$$I_g = b_1 J_1 + b_2\sqrt{J_2},$$
$$\tau_{eq}(\xi, \vartheta, \in^p) = c_2(\vartheta)(1 - \xi)\ln\frac{1}{\xi}\left\{2\kappa_s(\vartheta) - [\kappa_s(\vartheta) - \kappa_0(\vartheta)]\, F(\xi_0, \xi, \vartheta)\right\}, \tag{4.7}$$
$$c_1(\vartheta) = \text{const}, \qquad c_2(\vartheta) = \text{const},$$
$$F(\xi_0, \xi, \vartheta) = \left(\frac{\xi_0}{1 - \xi_0}\frac{1 - \xi}{\xi}\right)^{2/3(\delta)} + \left(\frac{1 - \xi}{1 - \xi_0}\right)^{2/3(\delta)}.$$

As in the infinitesimal theory of elasticity we assume linear properties of the material, i.e.

$$\mathcal{L}^e = 2\mu\mathbf{I} + \lambda(\mathbf{g} \otimes \mathbf{g}) \tag{4.8}$$

where μ and λ denote the Lamé constants, and the thermal expansion matrix is postulated as

$$\mathcal{L}^{th} = (2\mu + 3\lambda)\theta\mathbf{g}, \tag{4.9}$$

where θ is the thermal expansion constant.

4.2. Assumption of the material functions for an isothermal process

Let us assume the plastic potential function in the form

$$f = \left(J_2' + n\xi J_1^2\right)^{1/2}, \tag{4.10}$$

the isotropic hardening-softening function

$$\kappa = [\kappa_s - (\kappa_s - \kappa_0)\exp(-\delta \in^p)]\left[1 - \left(\frac{\xi}{\xi_F}\right)^{\beta}\right], \tag{4.11}$$

and the functions in the evolution equation for porosity

$$g^* = c_1 \frac{\xi}{1-\xi}, \qquad I_g = b_1 J_1 + b_2\sqrt{J_2'},$$

$$\tau_{eq}(\xi, \in^p) = c_2(1-\xi)\ln\frac{1}{\xi}\left[2\kappa_s - (\kappa_s - \kappa_0)\,F(\xi_0, \xi)\right], \tag{4.12}$$

$$F(\xi_0, \xi) = \left(\frac{\xi_0}{1-\xi_0}\frac{1-\xi}{\xi}\right)^{2/3(\delta)} + \left(\frac{1-\xi}{1-\xi_0}\right)^{2/3(\delta)}.$$

We keep the form of the overstress function as in (4.5).

4.3. Determination of the material constants

To determine the material constants assumed we take advantage of the experimental observations presented by CHAKRABARTI and SPRETNAK [2]. They investigated the localized fracture mode for tensile steel sheet specimens simulating both the plane stress and plane strain processes. The material used in their study was AISI 4340 steel. The principal variable in this flat specimen test was the width – to – thickness ratio. Variation in specimen geometry produces significant changes in the stress state, directions of shear bands, and ductility. They found that fracture propagated consistently along the shear band localized region.

Let us now consider the isothermal dynamic process for a thin steel plate under the condition of plane stress state, cf. DORNOWSKI and PERZYNA [8]. In fact we idealize the initial-boundary value problem investigated by CHAKRABARTI and SPRETNAK [2] by assuming the velocity-driven isothermal process for a thin steel plate. The problem has been solved by using the finite difference method.

In numerical calculations it is assumed:

$$\dot{V}_0 = 1.5 \text{ m/s}, \qquad t_0 = 50 \text{ μs}, \qquad t_f = 800 \text{ μs}. \tag{4.13}$$

The material of a plate is AISI 4340 steel.

Based on the best curve fitting of the experimental results obtained by CHAKRABARTI and SPRETNAK [2] for the stress-strain relation, the identification of the material constants has been done for both materials A and B, cf. Tables 1 and 2.

Table 1. Material A (plate).

$\rho_{\text{Ref}} = 7830$ kg/m^3	$E = 208$ GPa	$v = 0.3$	$\kappa_0 = 635$ MPa
$\kappa_s = 808$ MPa	$\delta = 28$	$\beta = 2.2$	$T_m = 0.001$ μs
$m = 1$	$c_1 = 0.202$	$c_2 = 0.067$	$b_1 = 1.0$
$b_2 = 1.3$	$\xi_0 = 6 \cdot 10^{-4}$	$\xi_F = 0.2$	$n = 0.25$

Table 2. Material B (cohesive band).

$\rho_{\text{Ref}} = 1190$ kg/m^3	$E = 3.24$ GPa	$v = 0.35$	$\kappa_0 = 5$ MPa
$\kappa_s = 92$ MPa	$\delta = 80$	$\beta = 2.0$	$T_m = 0.001$ μs
$m = 1$	$c_1 = 0.202$	$c_2 = 0.067$	$b_1 = 1.0$
$b_2 = 1.3$	$\xi_0 = 6 \cdot 10^{-4}$	$\xi_F = 0.09$	$n = 0.25$

Let us now assume the velocity-driven adiabatic process for a thin steel plate and proceed similarly as in the case of an isothermal process (cf. DORNOWSKI and PERZYNA [8]). Then the material constants for an adiabatic process for both materials A and B can be determined, cf. Tables 3 and 4.

Table 3. Material A (plate).

$\kappa_s^* = 808$ MPa	$\kappa_s^{**} = 230$ MPa	$\kappa_0^* = 635$ MPa	$\kappa_0^{**} = 181$ MPa
$\delta^* = 28$	$\delta^{**} = 8$	$\beta^* = 2.2$	$\beta^{**} = 0.63$
$\vartheta_0 = 293$ K	$\xi_F = 0.2$	$\rho_{\text{Ref}} = 7850$ kg/m^3	$E = 208$ GPa
$\nu = 0.3$	$\theta = 12 \cdot 10^{-6}$ K^{-1}	$T_m = 0.001$ μs	$m = 1$
$c_1 = 0.202$	$c_2 = 0.067$	$b_1 = 1.0$	$b_2 = 1.3$
$\xi_0 = 6 \cdot 10^{-4}$	$n = 0.25$	$\chi^* = 0.9$	$c_p = 455$ J/kg K

Table 4. Material B (cohesive band).

$\kappa_s^* = 92$ MPa	$\kappa_s^{**} = 26$ MPa	$\kappa_0^* = 5$ MPa	$\kappa_0^{**} = 1.5$ MPa
$\delta^* = 80$	$\delta^{**} = 22$	$\beta^* = 2.0$	$\beta^{**} = 0.57$
$\vartheta_0 = 293$ K	$\xi_F = 0.09$	$\rho_{Ref} = 1190$ kg/m^3	$E = 3.24$ GPa
$\nu = 0.35$	$\theta = 12 \cdot 10^{-6}$ K^{-1}	$T_m = 0.001$ μs	$m = 1$
$c_1 = 0.202$	$c_2 = 0.067$	$b_1 = 1.0$	$b_2 = 1.3$
$\xi_0 = 6 \cdot 10^{-4}$	$n = 0.25$	$\chi^* = 0.9$	$c_p = 455$ J/kg K

We can now determine the internal length-scale parameter for the case of one–dimensional wave propagation for both the materials assumed. For material A (plate) (i.e. AISI 4340 steel) we have $l = 3$ μm, and for material B (cohesive band) $l = 0.5$ μm.

5. Numerical solution of the initial boundary-value problems

5.1. Formulation of the initial boundary-value problem

We analyse isothermal and adiabatic processes for the thin flat specimen made of two identical elements (material A) joined by a band (material B), Fig. 6. Initial dimensions of the specimen are taken as follows: the height is equal 0.15 mm and width is 0.3 mm. The width of the cohesive band is 1 μm, so it is the mesoscale size range. In this cohesive band the initial notch 0.03 mm is localized symmetrically.

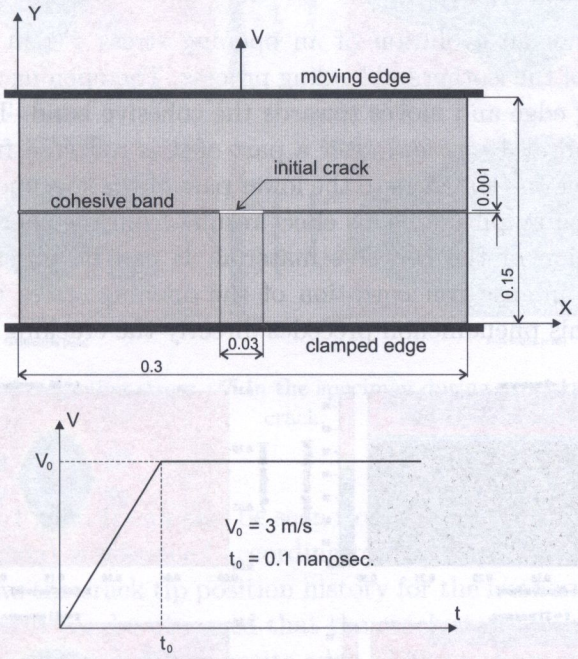

Fig. 6. Specimen geometry and its kinematical constraint (all dimensions are in millimeters).

It is assumed that the boundary conditions are modelled by the speed of the upper edge of the specimen, while the lower edge is clamped. The initial conditions of the problem are homogeneous.

A two-dimensional, plane stress, finite difference model for the entire specimen is applied. The regular mesh consists of a total of 45 000 nodes and the discretization parameters are $\Delta x = \Delta y = 1\mu\text{m}$, $\Delta t = 0.3685 \cdot 10^{-11}\text{s}$.

Both materials of the specimen are modelled as elastic-viscoplastic with isotropic hardening-softening effects.

It is assumed that the material softening is caused by the intrinsic microdamage mechanisms.

We have modelled the boundary by the velocity of nodes lying on the upper edge according to the relation

$$V(t) = V_0 t/t_0 \quad \text{for} \quad t \leq t_0 \qquad \text{and} \qquad V(t) = V_0 \quad \text{for} \quad t > t_0. \tag{5.1}$$

The numerical results are obtained for $V_0 = 3$ m/s and the rise time $t_0 = 10^{-10}$s.

The finite difference method with explicit time integration scheme (conditionally stable) is used. The elaborated algorithm satisfies the material objectivity principle with respect to any diffeomorphism (any motion).

5.2. Investigation of the macrocrack propagation along a bimaterial interface band

Figure 7 shows an evolution of an opening stress τ^{yy} in the specimen at several instants of the isothermal loading process. The opening stress wave starts from the loading edge and moves towards the cohesive band. This wave reaches the cohesive band at 15 ns and after a part of it is reflected from the interface band, and another one transfers to the lower part of the specimen simultaneously decreasing its own amplitude. This effect results from the energy dissipation on plastic deformation of the cohesive material. It can be observed from Fig. 7 that there is an intense concentration of the opening stress in the vicinity of the notch tip. This phenomenon precedes directly the cracking phase illustrated

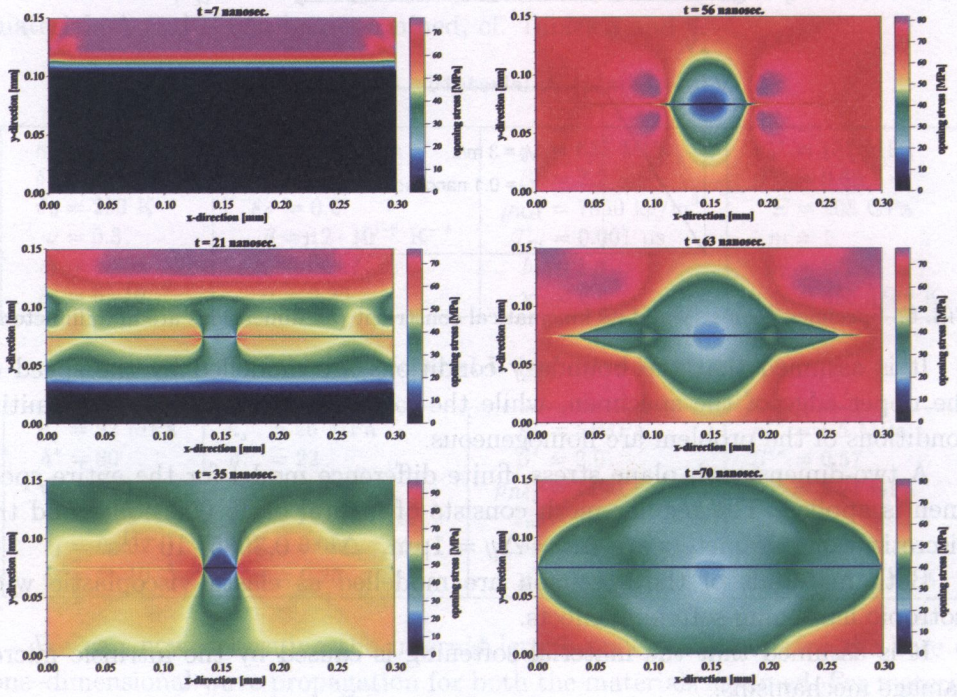

FIG. 7. Evolution of a opening stress τ^{yy} in the specimen at several instants of the isothermal loading process.

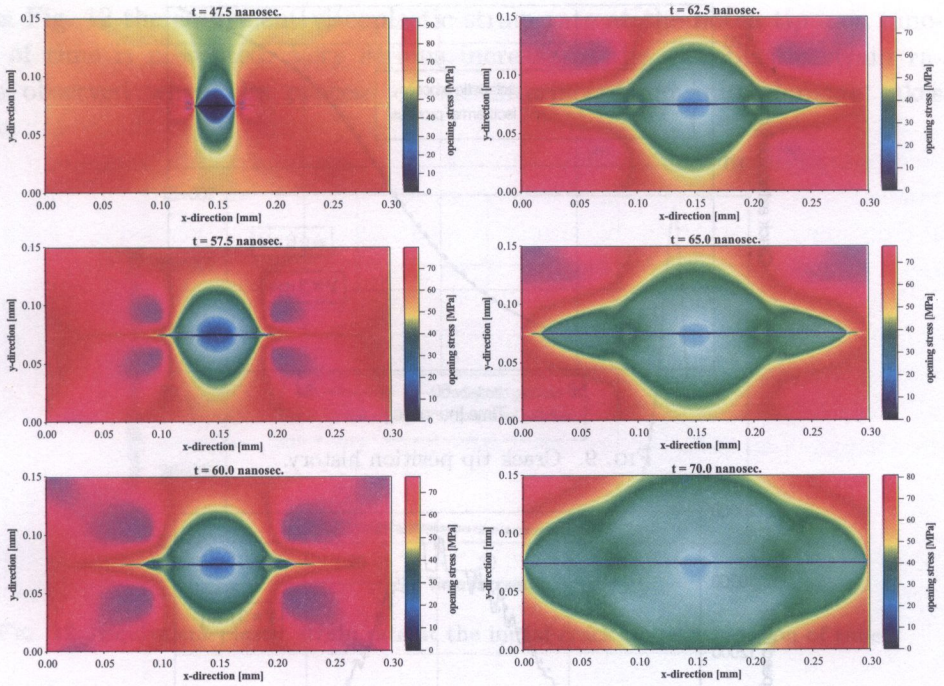

FIG. 8. Evolution of a opening stress τ^{yy} in the specimen during propagation of the interface crack.

most precisely in Fig. 8. It can also be seen from these figures that the unloading region (green region) is deepened according to the crack growth.

Figure 9 shows the crack tip position history for the isothermal and adiabatic loading processes. It can be observed that the crack starts from the initial crack tip from 53 ns and reaches the opposite edge at 68 ns. Also, it is clear from the above results that the effect of temperature is unimportant in this case.

The crack tip speed history is shown in Fig. 10. It is seen that for the crack extension to 80 μm the speed of cracking increases to 18 000 m/s, and then decreases to about 4 000 m/s. These values exceed many times the dilatational wave speed for the both materials. Some visible crack speed oscillations result from the wave interaction.

The evolution of the equivalent plastic strain in the node immediately ahead of the notch tip is displayed in Fig. 11. Here, the equivalent plastic deformation may be treated as a measure of the cohesive band deformability. This figure shows that the equivalent plastic strain evolves almost linearly during the time interval 15 to 40 ns and then evolves rapidly. It indicates that after 40 ns the intensity growth of microdamage takes place in the considered node. The equivalent plastic strain reaches its greatest value (about 3%) at the local fracture of a material.

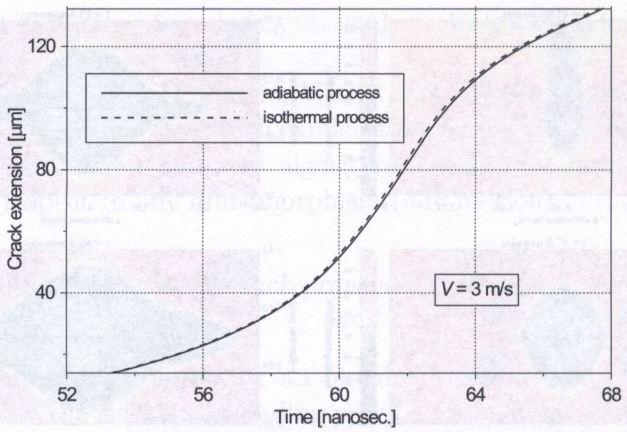

FIG. 9. Crack tip position history.

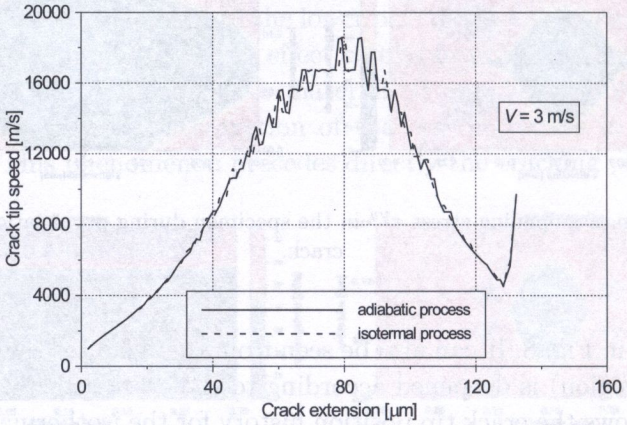

FIG. 10. Crack tip speed history.

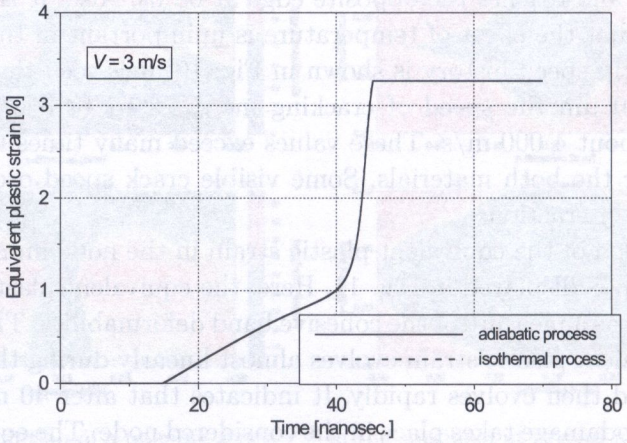

FIG. 11. Equivalent plastic strain at the initial crack tip as a function of time.

In Fig. 12 the equivalent viscoplastic strain rate at the notch tip as a function of time is presented. Very serious increase of the viscoplastic strain rate is observed when the process of the interface band microdamage takes place.

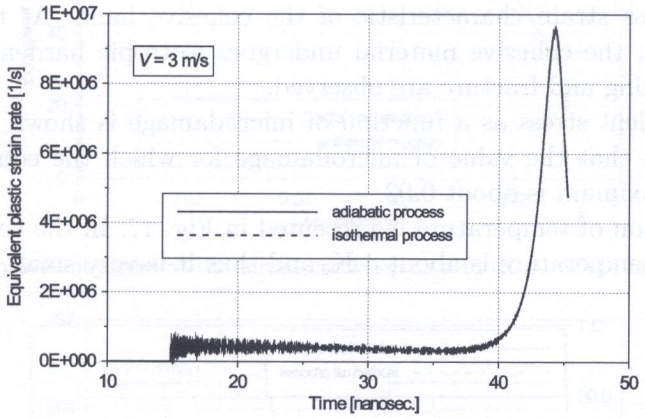

FIG. 12. Equivalent plastic strain rate at the initial crack tip as a function of time.

The corresponding variation of the equivalent stress ($\tau_e = \sqrt{\frac{2}{3}\boldsymbol{\tau}' : \boldsymbol{\tau}'}$) in time is presented in Fig. 13. It may be treated as an illustration of the cohesive band strength evolution rapture. The equivalent stress reaches its maximal value of 80 MPa at 40 ns, and then the softening of material can be observed. As a result, the cohesive band loses its carrying capacity and crack initiation takes place in 45 ns.

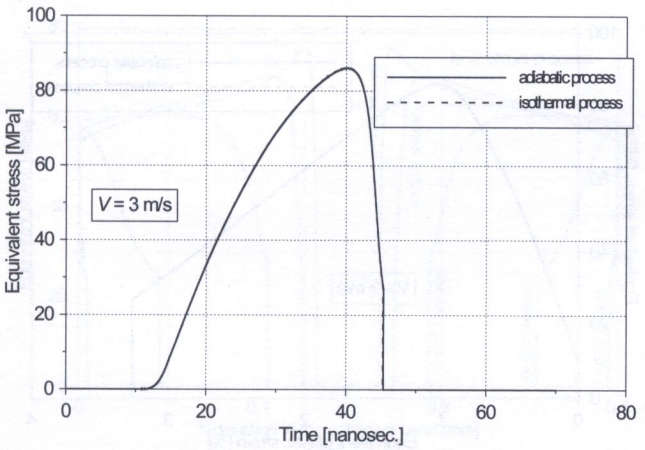

FIG. 13. Equivalent stress at the initial crack tip as a function of time.

An evolution of the microdamage parameter in the initial crack environment is shown in Fig. 14. From this figure, it can be observed that the void fraction reaches the prescribed failure value of $\xi_F = 0.09$ in 45 ns.

A dependence of the equivalent stress on the equivalent plastic strain at the considered node is presented in Fig. 15. This figure illustrates mainly the nonelastic stress–strain characteristic of the cohesive band. At the beginning of deformation, the cohesive material undergoes isotropic hardening, later the material softening and fracture are observed.

The equivalent stress as a function of microdamage is shown in Fig. 16. It can be noticed that the value of microdamage for which the equivalent stress reaches the maximum is about 0.02.

The evolution of temperature is presented in Fig. 17. In the considered case the change of temperature is about 4 K, and thus it is very small.

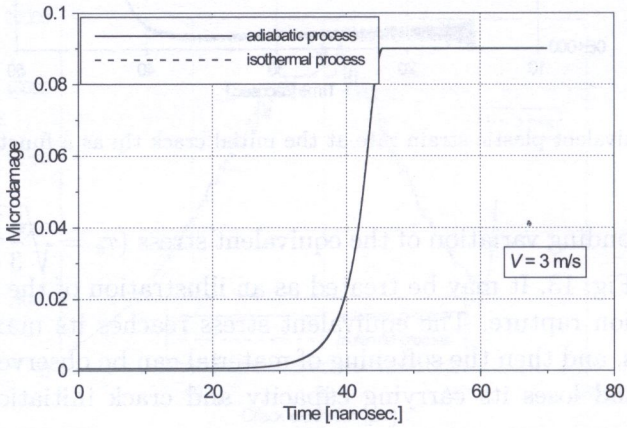

FIG. 14. Microdamage at the initial crack tip as a function of time.

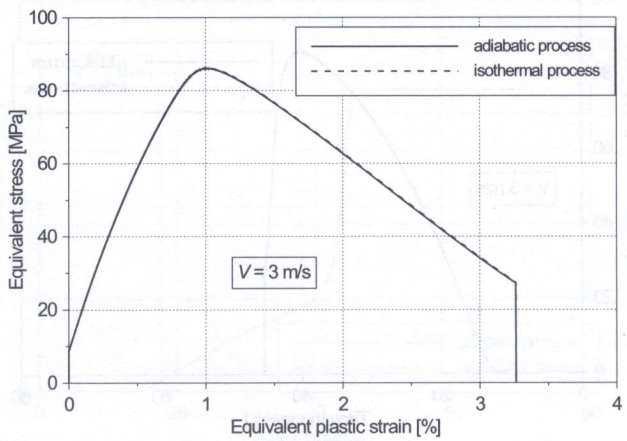

FIG. 15. Equivalent stress at the initial crack tip as a function of the equivalent plastic strain.

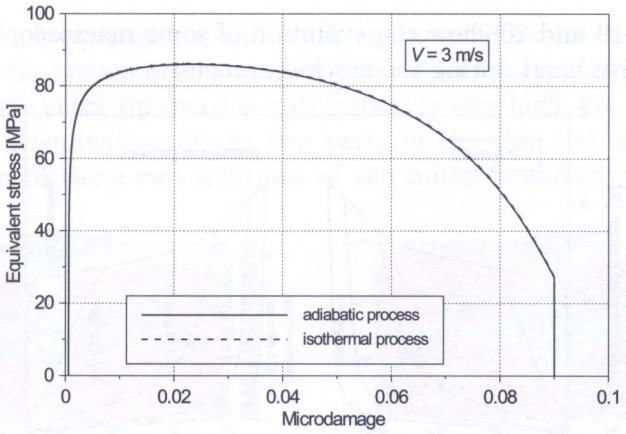

FIG. 16. Equivalent stress at the initial crack tip as a function of the microdamage.

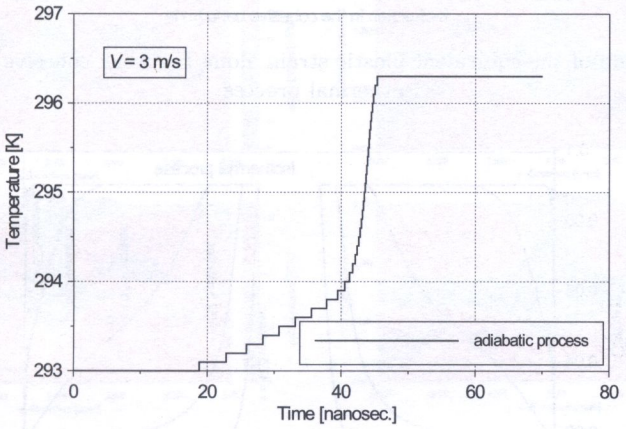

FIG. 17. Temperature at the initial crack tip as a function of time (adiabatic process).

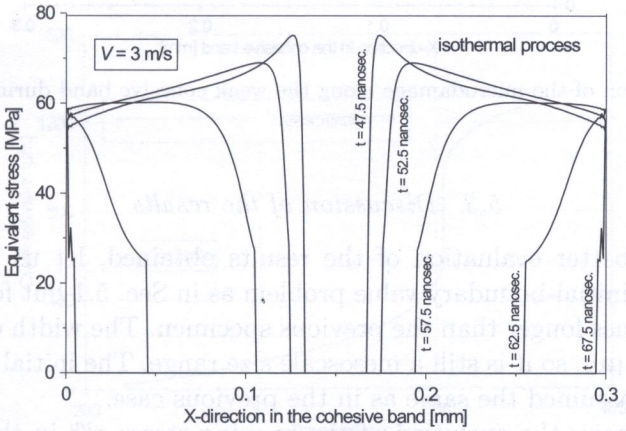

FIG. 18. Evolution of the equivalent stress along the weak cohesive band during an isothermal process.

Figures 18, 19 and 20 show the evolution of some macroscopic values along the weak cohesive band during the cracking process.

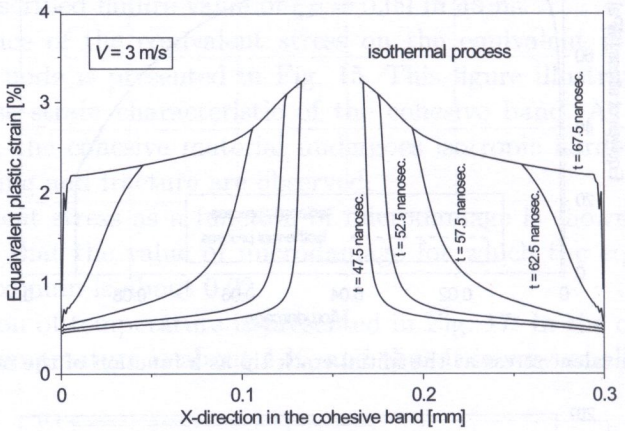

FIG. 19. Evolution of the equivalent plastic strain along the weak cohesive band during an isothermal process.

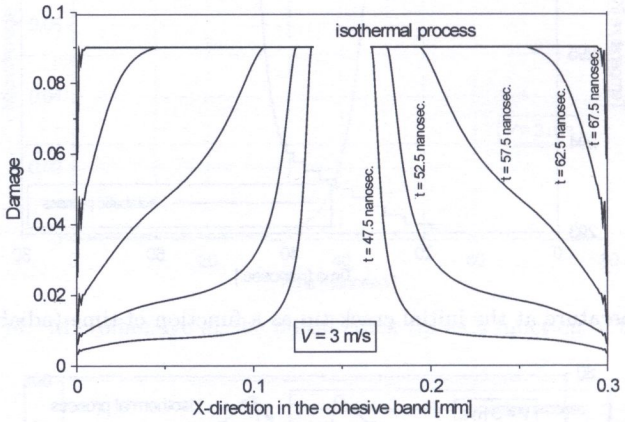

FIG. 20. Evolution of the microdamage along the weak cohesive band during an isothermal process.

5.3. Discussion of the results

To have a better evaluation of the results obtained, let us formulate and solve the same initial-boundary value problem as in Sec. 5.1 but for the thin flat specimen 10 times longer than the previous specimen. The width of the cohesive band is now 10 μm, so it is still a mesoscale size range. The initial and boundary conditions are assumed the same as in the previous case.

Figure 21 shows the evolution of the opening stress τ^{yy} in the specimen at several instants of the isothermal loading process considered. Figures 22 and

23 show the crack tip position and crack tip speed histories, respectively. We observe that at the instant of 360 nanosec we have very sharp increase of the crack extension and the crack tip speed at this instant is very high. So, we have almost instantaneous delamination of the two parts of the thin flat specimen. From the comparison of these two solutions of the initial-boundary value problems

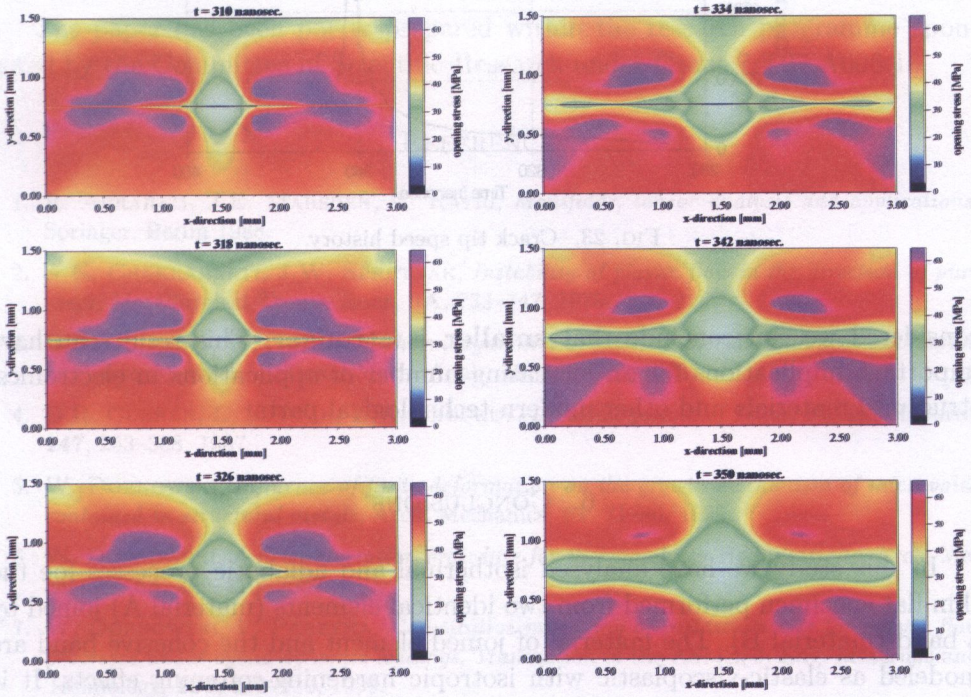

FIG. 21. Evolution of a opening stress τ^{yy} in the specimen at several instants of the isothermal process.

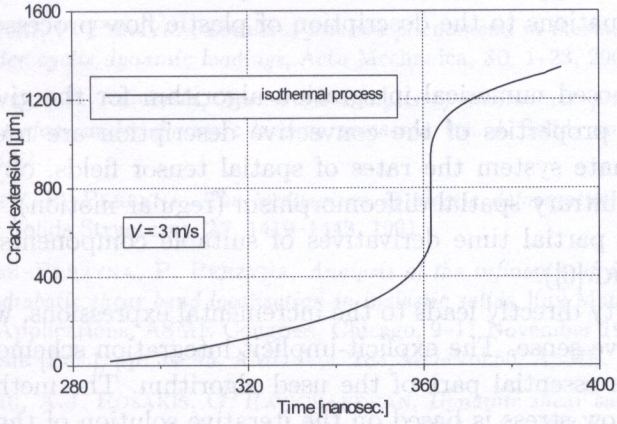

FIG. 22. Crack tip position history.

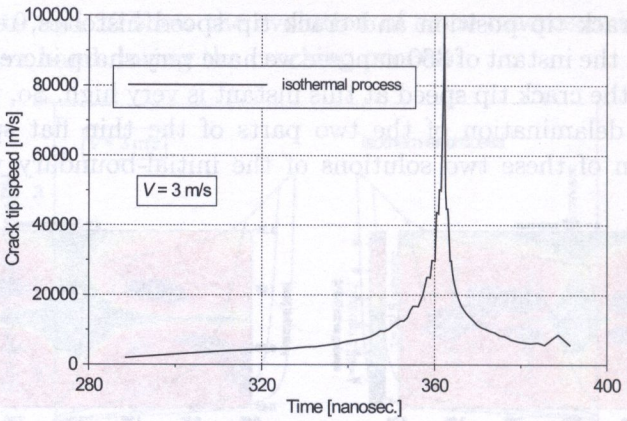

FIG. 23. Crack tip speed history.

considered we can conclude that **smaller is stronger**. This result can have important implications for an increasing number of applications in electronics, structural materials and other modern technological parts.

6. CONCLUSIONS

In this study we have analysed isothermal and adiabatic processes foe the thin flat specimen performed from two identical elements (material A) joined by a band (material B). The material of joined element and the cohesive band are modeled as elastic-viscoplastic with isotropic hardening-softening effects. It is assumed that the material softening is caused by intrinsic microdamage mechanism and temperature rise. The spatial description is assumed as physically most natural. Such an approach has also a reson, which results from application of constitutive equations to the description of plastic flow processes in the actual state.

In the proposed numerical integration algorithm for the given constitutive equations, the properties of the convective description are used. In the convective coordinate system the rates of spatial tensor fields, objective with respect to the arbitrary spatial diffeomorphism (regular motion), are represented by matrices of partial time derivatives of suitable components of these fields (cf. DORNOWSKI [6]).

This property directly leads to the incremental expressions, which are objective in the above sense. The explicit-implicit integration scheme for the plastic flow rule is the essential part of the used algorithm. The method of determination of the flow stress is based on the iterative solution of the dynamic yield condition with respect to the norm of the viscoplastic deformation tensor.

The numerical results have proven the usefulness of the presented constitutive theory and have shown, at least qualitatively, the type of crack speed histories and crack tip fields seen in the experiments.

Acknowledgment

The paper has been partly prepared within the research programme sponsored by the Committee of Scientific Research under Grant 7 T07 A006 16.

References

1. R. Abraham, J.E. Marsden, T. Ratiu, *Manifolds, tensor analysis and applications*, Springer, Berlin 1988.
2. A.K. Chakrabarti, J.W. Spretnak, *Instability of plastic flow in the direction of pure shear*, Metallurgical Transactions, **6A**, 733–747, 1975.
3. B.D. Coleman, W. Noll, *The thermodynamics of elastic materials with heat conduction and viscosity*, Arch. Rational Mech. Anal., **13**, 167–178, 1963.
4. D.R. Curran, L. Seaman, D.A. Shockey, *Dynamic failure of solids*, Physics Reports, **147**, 253–388, 1987.
5. W. Dornowski, *Influence of finite deformation on the growth mechanism of microvoids contained in structural metals*, Arch. Mechanics, **51**, 71–86, 1999.
6. W. Dornowski, *A new integration procedure for thermo-elasto-viscoplasticity*, Arch. Mechanics, **54**, 389–410, 2002.
7. W. Dornowski, P. Perzyna, *Constitutive modelling of inelastic solids for plastic flow processes under cyclic dynamic loadings*, Transaction of the ASME, J. Eng. Materials and Technology, **121**, 210–220, 1999.
8. W. Dornowski, P. Perzyna, *Localization phenomena in thermo-viscoplastic flow processes under cyclic dynamic loadings*, Computer Assisted Mechanics and Engineering Sciences, **7**, 117–160, 2000.
9. W. Dornowski, P. Perzyna, *Localized fracture phenomena in thermo-viscoplastic flow processes under cyclic dynamic loadings*, Acta Mechanica, **30**, 1–23, 2001.
10. W. Dornowski, P. Perzyna, *Numerical analysis of macrocrack propagation along a bimaterial interface under dynamic loading processes*, Int. J. Solids and Structures, **39**, 4949–4977, 2002.
11. M.K. Duszek, P. Perzyna, *The localization of plastic deformation in thermoplastic solids*, Int. J. Solids Structures, **27**, 1419–1443, 1991.
12. M.K. Duszek–Perzyna, P. Perzyna, *Analysis of the influence of different effects on criteria for adiabatic shear band localization in inelastic solids*, [in:] Material Instabilities: Theory and Applications, ASME Congress, Chicago, 9–11 November 1994, R.C. Batra and H.M. Zbib [Eds.], pp. 59–85, AMD–Vol. 183/MD–Vol.50, ASME, New York, 1994.
13. P.R. Guduru, A.J. Rosakis, G. Ravichandran, *Dynamic shear bands: an investigation using high speed optical and infrared diagnostic*, Mechanics of Materials, **33**, 371–402, 2001.

14. P.R. GUDURU, A.T. ZEHNDER, A.J. ROSAKIS, G. RAVICHANDRAN, *Dynamic full field measurements of crack tip temperatures*, Engineering Fracture Mechanics, **68**, 1535–1556, 2001.

15. J.N. JOHNSON, *Dynamic fracture and spallation in ductile solids*, J. Appl. Phys., **52**, 2812–2825, 1981.

16. J. LAMBROS, A. ROSAKIS, *Dynamic decohesion of bimaterials: Experimental observations and failure criteria*, Int. J. Solids Structures, **32**, 2677–2702, 1995.

17. J. LAMBROS, A. ROSAKIS, *Shear dominated transonic interfacial crack growth in a bimaterial – I. Experimental observations*, J. Mech. Phys. Solids, **43**, 169–188, 1995.

18. J. LAMBROS, A. ROSAKIS, *Shear dominated transonic interfacial crack growth in a bimaterial – II. Asymptotic fields and favorable velocity regimes*, J. Mech. Phys. Solids, **43**, 189–206, 1995.

19. T. ŁODYGOWSKI, P. PERZYNA, *Localized fracture of inelastic polycrystalline solids under dynamic loading processes*, Int. J. Damage Mechanics, **6**, 364–407, 1997.

20. J.E. MARSDEN, T.J.R. HUGHES, *Mathematical Foundations of Elasticity*, Prentice–Hall, Englewood Cliffs, New York 1983.

21. A. NEEDLEMAN, A.J. ROSAKIS, *The effect of bound strength and loading rate on the conditions governing the attainment of intersonic crack growth along interfaces*, J. Mech. Phys. Solids, **47**, 2411–2449, 1999.

22. J.A. NEMES, J. EFTIS, *Constitutive modelling of the dynamic fracture of smooth tensile bars*, Int. J. Plasticity, **9**, 243–270, 1993.

23. J. OLDROYD, *On the formulation of rheological equations of state*, Proc. R. Soc. Lond., **A200**, 523–541, 1950.

24. P. PERZYNA, *The constitutive equations for rate sensitive plastic materials*, Quart. Appl. Math., **20**, 321–332, 1963.

25. P. PERZYNA, *Fundamental problems in viscoplasticity*, Advances in Applied Mechanics, **9**, 343–377, 1966.

26. P. PERZYNA, *Thermodynamic theory of viscoplasticity*, Advances in Applied Mechanics, **11**, 313–354, 1971.

27. P. PERZYNA, *Constitutive modelling of dissipative solids for postcritical behaviour and fracture*, ASME J. Eng. Materials and Technology, **106**, 410-419, 1984.

28. P. PERZYNA, *Internal state variable description of dynamic fracture of ductile solids*, Int. J. Solids Structures, **22**, 797-818, 1986.

29. P. PERZYNA, *Constitutive modelling for brittle dynamic fracture in dissipative solids*, Arch. Mechanics, **38**, 725–738, 1986.

30. P. PERZYNA, *Interactions of elastic-viscoplastic waves and localization phenomena in solids*, IUTAM Symposium on Nonlinear Waves in Solids, August 15–20, 1993, Victoria, Canada; J.L. WEGNER and F.R. NORWOOD [Eds.], pp. 114–121, ASME 1995.

31. P. PERZYNA, A. DRABIK, *Description of micro-damage process by porosity parameter for nonlinear viscoplasticity*, Arch. Mechanics, **41**, 895–908, 1989.

32. A.J. ROSAKIS, G. RAVICHANDRAN, *Dynamic failure mechanics*, Int. J. Solids Structures, **37**, 331–348, 2000.

33. A.J. ROSAKIS, O. SAMUDRALA, D. COKER, *Cracks faster than the shear wave speed*, California Institute of Technology, SM Report 98–17, December 1998, 1998.

34. A.J. ROSAKIS, O. SAMUDRALA, D. COKER, *Cracks faster than the shear wave speed*, Science, **284**, 1337–1340, 1999.

35. S. SHIMA, M. OYANE, *Plasticity for porous solids*, Int. J. Mech. Sci., **18**, 285–291, 1976.

36. D.A. SHOCKEY, L. SEAMAN, D.R. CURRAN, *The microstatistical fracture mechanics approach to dynamic fracture problem*, Int. J. Fracture, **27**, 145–157, 1985.

37. D. SIDEY, L.F. COFFIN, *Low-cycle fatigue damage mechamisms at high temperature*, [in:] Fatigue Mechanisms, Proc. ASTM STP 675 Symposium, Kansas City, Mo., May 1978, J.T. Fong [Ed.], pp. 528–568, Baltimore 1979.

38. C. TRUESDELL, W. NOLL, *The Non-linear field theories of mechanics*, [in:] Handbuch der Physik III/3, S. FLÜGGE [Ed.], Springer–Verlag, Berlin 1965.

Received December 14, 2005; revised version May 11, 2006.